15. T. Hogg, B. A. Huberman, C. Williams, *Artif. Intell.* **81**, 1 (1996); S. Kirkpatrick and B. Selman, *Science* **264**, 1297 (1994).
16. T. Hogg and C. P. Williams, in *Proceedings of the Twelfth National Conference on Artificial Intelligence* (AAAI Press, Menlo Park, CA, 1994), pp. 331–336.
17. I. Gent and T. Walsh, *Artif. Intell.* **81**, 59 (1996); B. Selman and S. Kirkpatrick, *ibid.*, p. 273.
18. S. H. Clearwater, B. A. Huberman, T. Hogg, *Science* **254**, 1181 (1991); D. Aldous and U. Vazirani, in *Proceedings of the 35th Symposium on the Foundations of Computer Science*, S. Goldwasser, Ed. (IEEE Press, Los Alamitos, CA, 1994), pp. 492–501; N. Cesa-Bianchi *et al.*, in *Proceedings of the 25th Annual ACM Symposium on the Theory of Computing* (Association for Computing Machinery, New York, 1993), pp. 382–391.
19. T. Hogg and C. P. Williams, in *Proceedings of the Eleventh National Conference on Artificial Intelligence* (AAAI Press, Menlo Park, CA, 1993), pp. 231–236.
20. G. Roumeliotis and B. A. Huberman, in preparation.
21. L. K. Grover, in *Proceedings of the 28th Annual Symposium on the Theory of Computing* (Association for Computing Machinery, New York, 1996), pp. 212–219.
22. M. Boyer, G. Brassard, P. Hoyer, A. Tapp, in *Proceedings of the Workshop on Physics and Computation (PhysComp96)*, in press.
23. R.M.L. acknowledges the support of a Citibank fellowship at Stanford University.

9 August 1996; accepted 28 October 1996

Femtosecond Dynamics of Excited-State Evolution in $[Ru(bpy)_3]^{2+}$

Niels H. Damrauer, Giulio Cerullo,* Alvin Yeh, Thomas R. Boussie, Charles V. Shank, James K. McCusker†

Time-resolved absorption spectroscopy on the femtosecond time scale has been used to monitor the earliest events associated with excited-state relaxation in tris-(2,2′-bipyridine)ruthenium(II). The data reveal dynamics associated with the temporal evolution of the Franck-Condon state to the lowest energy excited state of this molecule. The process is essentially complete in ~300 femtoseconds after the initial excitation. This result is discussed with regard to reformulating long-held notions about excited-state relaxation, as well as its implication for the importance of non-equilibrium excited-state processes in understanding and designing molecular-based electron transfer, artificial photosynthetic, and photovoltaic assemblies in which compounds of this class are currently playing a key role.

Many of the photochemical and photophysical properties of molecules depend upon the kinetics of excited-state processes that occur after the absorption of a photon. Therefore, it is important to understand how excited states behave as a function of time. The conventional view of this temporal evolution holds that photoreactivity is largely dictated by the characteristics of the lowest energy excited state of a molecule. Thus, higher energy excited states are presumed to convert to this lowest energy state and in so doing are removed from any functional role in photochemical and photophysical transformations. Femtosecond time-resolved spectroscopy (*1*) has resulted in experimental observations that call into question the validity of this model; striking examples include the 200-fs *cis*-to-*trans* isomerization of rhodopsin (*2*), rapid photodissociation of CO from myoglobin-CO (*3*), and ultrafast electron injection into dye-sensitized semiconductor electrodes (*4*). These cases among others reveal a pattern of photoreactivity arising from nonthermalized excited states in which structural rearrangement and electron transfer can kinetically compete with processes such as intramolecular vibrational relaxation (IVR), internal conversion (IC), and intersystem crossing (ISC).

The inference that nonequilibrated excited states can play a chemically significant role in photoinduced transformations could have important consequences in a variety of areas ranging from design principles for electron-transfer assemblies and photochemical energy storage devices to the formulation of new theoretical models for molecular-based energy conversion and excited-state relaxation dynamics. Although much of the work in the ultrafast dynamics community has concentrated on either small molecules or biological systems, our research focuses on transition metal compounds (*5*, *6*). Considerable effort is being expended in many laboratories to incorporate such complexes into schemes for artificial photosynthesis (*7*), photocatalysis (*8*), and the development of molecular-based photovoltaic and opto-electronic devices (*9*). In addition, the importance of ISC and IC processes in the photoinduced properties of metal-containing complexes makes such systems of interest for ultrafast dynamical studies of their excited-state behavior (*10*). We have obtained results that are not consistent with conventional models for describing photoinduced dynamics in transition metal complexes, suggesting the need to reevaluate currently accepted views of their excited-state behavior.

Tris-(2,2′-bipyridine)ruthenium(II), or $[Ru(bpy)_3]^{2+}$,

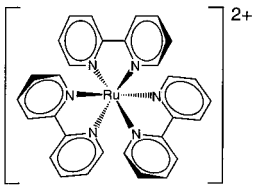

is representative of a class of molecules that has played a central role in the development of inorganic photophysics in addition to providing the underpinning for the last two decades of research on transition metal–based photosensitization, charge separation, and photoinduced electron transfer chemistry (*11*). We have therefore chosen it as a prototype for our study of the ultrafast dynamics of metal complexes. The strong visible absorption characteristic of this molecule (Fig. 1) can be described as a metal-to-ligand charge transfer ($^1MLCT \leftarrow {}^1A_1$), in which an electron located in a metal-based *d*-orbital is transferred to a π^* orbital of one of the bpy ligands ($h\nu$, photon energy) (*12*). The excited-state species that is eventually

$$[Ru^{II}(bpy)_3]^{2+} \xrightarrow{h\nu} [Ru^{III}(bpy^-)(bpy)_2]^{2+}$$

formed (a ^3MLCT state) is well known to engage in both oxidative and reductive chemistry (*11*). This capability, coupled with its relatively long lifetime in fluid solution ($\tau \approx 1$ μs), near unity quantum yield of formation (*13*), the high visible absorptive cross section of the ground state, and the overall photochemical stability of this molecule and its derivatives makes them amenable to a wide variety of applications (*14*, *15*). We have used femtosecond absorption spectroscopy to time resolve the formation of the ^3MLCT state in $[Ru(bpy)_3]^{2+}$ (*16*) and have observed the initial evolution of the Franck-Condon state.

The laser system used has been described in detail elsewhere (*17*, *18*). Excited-state difference spectra at various time delays Δt (Fig. 2) show that spectral changes in the 450- to 490-nm range are quite dramatic: A bleach begins to evolve at $\lambda = 470$ nm near

N. H. Damrauer, T. R. Boussie, J. K. McCusker, Department of Chemistry, University of California, Berkeley, CA 94720, USA.
G. Cerullo and A. Yeh, Material Sciences Division, Lawrence Berkeley National Laboratory, Berkeley, CA 94720, USA.
C. V. Shank, Department of Chemistry, University of California, Berkeley, CA 94720, and Materials Science Division, Lawrence Berkeley National Laboratory, Berkeley, CA 94720, USA.
*Present address: Dipartimento di Fisica del Politecnico, P.za L. Da Vinci 32, 20133 Milano, Italy.
†To whom correspondence should be addressed.

$\Delta t = 0$ fs and grows substantially in intensity by $\Delta t = 50$ fs along with what appears to be a weak excited-state absorption at higher energy. The transient exhibits both a marked blue shift and changes in its spectral profile in all of the early time data until $\Delta t \approx 300$ fs, after which most of this spectral shifting appears to have ceased. Single-wavelength kinetics traces, which were obtained by passing the probe beam through a monochromator after the sample, likewise show the growth of a bleach signal in the 450- to 490-nm region for the first 200 to 300 fs as well as a very weak excited-state absorption for $\lambda > 500$ nm. These changes at early times are complete at all wavelengths for $\Delta t > 300$ fs, consistent with the spectral traces illustrated in Fig. 2. Given that the lifetime of the ^{3}MLCT state under these experimental conditions is on the order of 1 μs, the most critical aspect of the femtosecond difference spectra with regard to the formation of the ^{3}MLCT state is the point at which the spectra stop changing. The data show that this occurs by ~300 fs after the initial excitation: There is no evidence of any additional significant changes in the absorptive properties of the molecule in the spectra collected from $\Delta t = 300$ fs to 5 ps.

We verified that the spectrum established by $\Delta t = 300$ fs corresponds to that of the ^{3}MLCT state by obtaining nanosecond time-resolved data. The details of the laser spectrometer used to collect these data will be published elsewhere (*19*). The excited-state–ground-state absorption difference spectrum for $[Ru(bpy)_3]^{2+}$ in CH_3CN obtained from this experiment is illustrated in Fig. 3A. Excited-state–ground-state isosbestic points (that is, the change in absorbance $\Delta A = 0$) present at 400 and 500 nm and the strong bleach in the 400- to 500-nm range are characteristic of the thermalized ^{3}MLCT state (*20*). An overlay of the difference spectra collected at $\Delta t = 500$ fs and 5 ps with the nanosecond data collected on $[Ru(bpy)_3]^{2+}$ in the region from 440 to 520 nm (Fig. 3B) shows that the three spectra are essentially superimposable within the noise level of the femtosecond data; the mismatch in the spectra at $\lambda < 450$ nm is likely because of the decreased signal-to-noise ratio in this region for the femtosecond data (see caption to Fig. 2). The comparison in Fig. 3B in conjunction with the data presented in Fig. 2 provides strong evidence that the excited state probed on the nanosecond time scale and at $\Delta t > 300$ fs are the same. Unfortunately, the weak nature of the excited-state absorption for $\lambda > 500$ nm makes it difficult to observe the isosbestic cleanly in the femtosecond transient spectra, but the single-wavelength traces verify its presence. This result provides additional support for our assignment, as we consider it extremely unlikely that additional states would have an isosbestic point coincident with the $^1A_1$/^{3}MLCT isosbestic of $[Ru(bpy)_3]^{2+}$ and show the same absorption profile. All of the kinetic and spectroscopic data are therefore consistent with the system being essentially established in the ^{3}MLCT state in ~300 fs, implying a half-life for the formation of this state on the order of 100 fs.

The complex evolution of the spectra between $\Delta t = 0$ and 300 fs evident from the

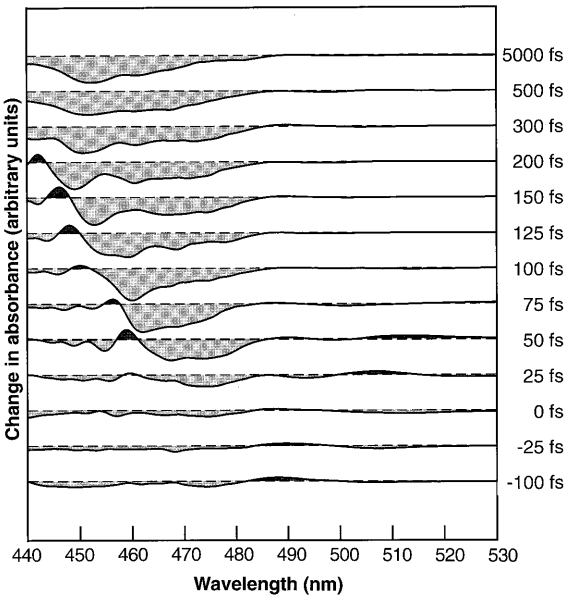

Fig. 2. Femtosecond time-resolved excited-state–ground-state absorption difference spectra for $[Ru(bpy)_3](PF_6)_2$ in CH_3CN solution at 298 K (*17*). The probe pulse gave adequate intensity for probing in the 450- to 530-nm range; below 450 nm, the relative amplitude of the signal dropped due to the vanishing intensity of the probe pulse in this region and the strong ground-state absorbance of the sample. The resulting poor signal-to-noise ratio resulted in some uncertainty in the baseline correction and hence the amplitude of the differential absorption in this portion of the spectrum. The orientation of the probe beam was set at the magic angle (~55°) relative to the parallel pump beam to minimize polarization effects. Detection was accomplished with an optical multichannel analyzer (OMA), and wavelength calibration was verified with a HeNe laser. The time delays were effected with an optical delay line. The position of $\Delta t = 0$, defined as the maximum of the pump-probe cross correlation, was checked both before and after each full scan, and in no case was the drift over the course of the experiment greater than ~5 fs. The dotted line in each spectrum corresponds to $\Delta A = 0$, and the inset numbers indicate probe beam delay times from $\Delta t = 0$. The data were smoothed with a gaussian smoothing function with a bandwidth of 2 nm; a somewhat broader filter was applied to the data between 470 and 480 nm to compensate for an artifact associated with the OMA.

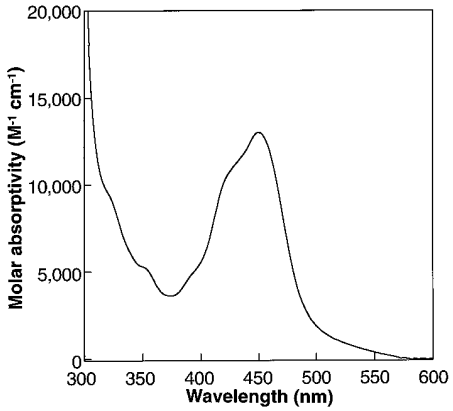

Fig. 1. Electronic absorption spectrum of $[Ru(bpy)_3](PF_6)_2$ in CH_3CN solution at 298 K.

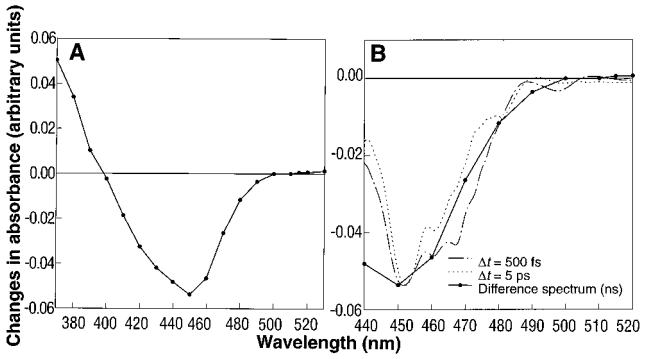

Fig. 3. (**A**) Excited-state–ground-state absorption difference spectrum of $[Ru(bpy)_3](PF_6)_2$ in CH_3CN following nanosecond excitation at 475 nm. The spectrum was obtained point-by-point by plotting the amplitude from a single-exponential fit of the excited-state relaxation data as a function of probe wavelength. The absorptive feature in the ultraviolet (λ_{max} = 370 nm) is due to ligand-based transitions of the bpy^- chromophore. The bleach in the region from ~400 to 500 nm is a superposition of absorptions associated with the ^{3}MLCT state and loss of the strong ground state ^{1}MLCT ← $^1A_1$ absorption. Extremely weak absorptive features for $\lambda > 500$ nm are due either to bpy^- transitions or LMCT transitions of the Ru^{III} excited-state chromophore. (**B**) Overlay of the spectrum of $[Ru(bpy)_3]^{2+}$ obtained at $\Delta t = 500$ fs and 5 ps after femtosecond excitation with the absorption difference spectrum of the compound after nanosecond excitation.

data in Fig. 2 indicate that there are dynamic processes occurring prior to the establishment of the long-lived excited state. The shift of the transient tracks the formation and thermalization (*21*) of the long-lived excited state. The overall spectral evolution of the signal is somewhat difficult to interpret in terms of molecular dynamics because it represents a superposition of both ground-state depletion and excited-state absorption or absorptions. Although we anticipate that the ground-state bleach will be instantaneous, excited-state features and hence the superposition spectrum will evolve as the molecule relaxes. The undulations that are apparent superimposed on the bleach signal and at shorter wavelengths do not appear in the solvent blank and therefore must be due to the sample. At present, we are uncertain as to the origin of these features. In terms of solvent contributions to the overall relaxation process, Fleming and co-workers (*22*) among others (*23*) have described the ultrafast molecular dynamics of CH_3CN in detail and showed that the inertial contribution to the solvent response of CH_3CN occurs on the 100-fs time scale. Therefore, given the time scale on which our spectra are changing and that the charge-transfer transition results in the formation of an excited state with a large dipole (*24*), solvent dynamics are likely having a profound influence on the intramolecular excited-state dynamics and, consequently, the spectral features at early times. In addition, IVR is undoubtedly occurring concurrent with solvent reorganization and ISC and may be contributing to changes in spectral profiles as well.

Although the details pertaining to the earliest time scale response in this system are not yet completely understood, the overall time scale for the formation of the ^{3}MLCT state has important implications for understanding the photoinduced dynamics of these types of systems. The first of these relates to the models which have been developed for describing excited-state relaxation (*5*, *6*). It is tacitly assumed that the fastest process occurring in the course of excited-state relaxation is IVR, then IC, then finally ISC: the rate constants for intramolecular relaxation are therefore ordered as $k_{IVR} \gg k_{IC} \gg k_{ISC}$. This anticipated trend is largely based upon the spin-allowed nature of IC versus the spin-forbidden ISC, as well as the expectation that the surface-to-surface crossings characteristic of both IC and ISC will be slower than single-surface processes such as IVR. The net result is a model that invokes a kind of relaxation cascade through the various excited electronic states of the system, with the excitation wave packet sampling the various potential energy surfaces that lie between the Franck-Condon state and the lowest energy excited state of the molecule.

However, the rapid formation of the ^{3}MLCT state after $^1\text{MLCT} \leftarrow {}^1A_1$ excitation appears to necessitate motion of the wave packet away from the Franck-Condon region directly to a region of overlap between the initial ^{1}MLCT and final ^{3}MLCT states; the observed time scale dictates that this likely occurs without significant evolution on the initial surface. We therefore suggest that the results of our femtosecond measurements on $[Ru(bpy)_3]^{2+}$ preclude the possibility of there being any well-defined establishment of the wave packet on any potential energy surface other than the lowest energy ^{3}MLCT state in the course of excited-state relaxation. Further support of this notion may come from the absence of vibrational coherence in the single-wavelength time traces, although this result may also be a consequence of the large number of modes in the molecule or that intramolecular relaxation occurs through coupling to high-frequency modes such that the oscillations are not temporally resolvable (*25*). To the extent that such processes as IVR, IC, and ISC can be distinguished from each other on these time scales (which may not be the case), our data suggest that all of these processes are occurring in concert with each other and with solvent reorganization as the system evolves in time. We believe that this represents a significant change in the conventional model for excited-state relaxation, one in which excited-state evolution is best described in terms of a direct transition from the initial surface to the final surface as opposed to a cascade through various well-defined vibronic levels of the system (*26*). Such intermediate energy levels may be present, but the wave packet only becomes stationary in the lowest energy vibronic state of the system in the course of excited-state relaxation.

Our results add to a growing body of evidence which shows that non-equilibrated excited states are of fundamental importance in the relaxation dynamics of transition metal complexes. We believe the details of many photophysical processes and indeed the identity and distribution of photoproducts are likely being determined in the earliest moments after photoexcitation (*27*). This leads to an important final point concerning how one might use this information in the design of molecular-based photolytic assemblies. The idea that dynamics other than intramolecular relaxation can occur prior to excited-state thermalization suggests that it might be possible to access the stored energy in the absorptive state to carry out photoinduced transformations. Such systems would have vastly improved efficiencies because intramolecular energy redistribution is largely responsible for reducing the quantum yields of most photochemical and photophysical processes. This may be what is occurring in many electron donor-acceptor complexes, for example, evidenced by the fact that the initial charge separation is generally too fast to be observed on the picosecond time scale. We suggest that the nature of molecular systems at or near the Franck-Condon state can play an important if not dominant role in photoinduced dynamics, and therefore should be considered in both the analysis of photophysical processes as well as the design of photochemical assemblies that incorporate transition metal complexes.

REFERENCES AND NOTES

1. For a recent survey of research in this area, see *Ultrafast Phenomena*, *Conference Edition*, volume 8 of the *Technical Digest Series* (Optical Society of America, San Diego, 1996).
2. L. A. Peteanu, R. W. Schoenlein, Q. Wang, R. A. Mathies, C. V. Shank, *Proc. Natl. Acad. Sci. U.S.A.* **90**, 11762 (1993).
3. J. C. Owrutsky, M. Li, R. M. Hochstrasser, *J. Phys. Chem.* **99**, 4842 (1995) and references therein.
4. J. R. Durrant, Y. Tachibana, J. Moser, M. Grätzel, D. R. Klug, in (*1*), pp. 140–141; J. M. Rehm, *et al*., *J. Phys. Chem.* **100**, 9577 (1996); H. Tributsch and F. Willig, *Sol. Energy Mater. Sol. Cells* **38**, 355 (1995) and references therein; R. Eichberger and F. Willig, *Chem. Phys.* **141**, 159 (1990).
5. For general references on inorganic photochemistry, see D. M. Roundhill, *Photochemistry and Photophysics of Metal Complexes* (Plenum, New York, 1994) and (*6*).
6. G. J. Ferraudi, *Elements of Inorganic Photochemistry* (Wiley, New York, 1988); H. Yersin and A. Vogler, Eds., *Photochemistry and Photophysics of Coordination Compounds* (Springer-Verlag, Berlin, 1987); A. Adamson and P. D. Fleischauer, Eds., *Concepts in Inorganic Photochemistry* (Wiley, New York, 1975).
7. T. J. Meyer, *Acc. Chem. Res.* **22**, 163 (1989); D. Gust and T. A. Moore, *Top. Curr. Chem.* **59**, 103 (1991); I. Willner and B. Willner, *ibid*., p. 153.
8. K. Kalyanasundaram and M. Grätzel, Eds., *Photosensitization and Photocatalysis Using Inorganic and Organometallic Compounds* (Kluwer Academic, Boston, 1993); G. L. McLendon, in *Photochemical Energy Conversion. Proceedings from the International Conference on Photochemical Conversion and Solar Energy Storage* (Elsevier, New York, 1989).
9. M. Grätzel and K. Kalyanasundaram, *Curr. Sci.* **66**, 706 (1994); M. Grätzel, *Renewable Energy* **5**, 118 (1994); V. Balzani and F. Scandola, in *Supramolecular Photochemistry* (Horwood, Chichester, UK, 1991); C. Jay, F. Groliere, O. Kahn, J. Krober, *Mol. Cryst. Liq. Cryst. Ser. A* **234**, 255 (1993) and references therein.
10. For representative studies of ultrafast dynamics involving transition metal compounds, see N. Serpone and M. A. Jamieson, *Coord. Chem. Rev.* **93**, 87 (1989); P. J. Reid, C. Silva, P. F. Barbara, L. Kark, J. T. Hupp, *J. Phys. Chem.* **99**, 2609 (1995); X. Q. Song *et al*., *ibid.* **97**, 3225 (1993); K. Tominaga, D. A. V. Kliner, A. E. Johnson, N. E. Levinger, P. F. Barbara, *J. Chem. Phys.* **98**, 1228 (1993) and references therein; S. K. Doorn, R. B. Dyer, P. O. Stoutland, W. H. Woodruff, *J. Am. Chem. Soc.* **115**, 6398 (1993), and references therein; S. M. Arrivo, T. P. Dougherty, T. P. Grubbs, E. J. Heilweil, *Chem. Phys. Lett.* **235**, 247 (1995); E. Lindsay, A. Vlcek Jr., C. H. Langford, *Inorg. Chem.* **32**, 3822 (1993); J. Vichova, F. Hartl, A. Vlcek Jr., *J. Am. Chem. Soc.* **114**, 10903 (1992).
11. For a recent overview of this area, see chap. 5 in (*5*). Other representative examples include A. Juris *et al*., *Coord. Chem. Rev.* **84**, 85 (1988); P. Besler *et al*., *J. Am. Chem. Soc.* **115**, 4076 (1993); E. H. Yonemoto

et al., *ibid.* **116**, 10557 (1994); J. D. Petersen, S. L. Gahan, S. C. Rasmussen, S. E. Ronco, *Coord. Chem. Rev.* **132**, 15 (1994).
12. For a recent computational analysis of the electronic structure of $[Ru(bpy)_3]^{2+}$, see C. Daul, E. J. Baerends, P. Vernooijs, *Inorg. Chem.* **33**, 3538 (1994).
13. J. N. Demas and A. W. Adamson, *J. Am. Chem. Soc.* **93**, 1800 (1971) and references therein.
14. S. L. Larson, C. M. Elliott, D. F. Kelley, *J. Phys. Chem.* **99**, 6530 (1995); D. G. Johnson, *et al*., *J. Am. Chem. Soc.* **115**, 5692 (1993); E. Danielson, C. M. Elliot, J. W. Merkert, T. J. Meyer, *ibid.* **109**, 2519 (1987); J. C. Sauvage *et al*., *Chem. Rev.* **94**, 993 (1994) and references therein.
15. B. O'Regan and M. Grätzel, *Nature* **353**, 737 (1991); T. J. Meyer *et al*., *Inorg. Chem.* **33**, 3952 (1994).
16. This system has been examined on the picosecond time scale by several researchers. See T. Yabe *et al*., *J. Phys. Chem.* **94**, 7128 (1990); Y. J. Chang *et al*., *ibid*., p. 729 and references therein; R. A. Malone and D. F. Kelley, *J. Chem. Phys.* **95**, 8970 (1991); L. F. Cooley, P. Bergquist, D. F. Kelley, *J. Am. Chem. Soc.* **112**, 2612 (1990). See also (*20*).
17. The laser spectrometer consists of a colliding-pulse mode-locked dye laser generating 60-fs pulses at 620 nm. The pulses are amplified to microjoule energies in a four-pass dye amplifier pumped at 540 Hz by the second harmonic of a Nd:yttrium-aluminum garnet (Nd:YAG) laser. The amplified pulses are focused through an ethylene glycol jet to generate a white light continuum. A portion of the continuum is then selected for further amplification in a second amplifier by the appropriate choice of dye. For more details, see R. W. Schoenlein, J. Y. Bigot, M. T. Portella, C. V. Shank, *Appl. Phys. Lett.* **58**, 801 (1991). For the experiments on $[Ru(bpy)_3]^{2+}$, Coumarin 480 was pumped by the third harmonic of the Nd:YAG to yield 25-fs pulses centered at 475 nm (full-width at half-maximum of 20 nm). A small portion of this pulse was redirected into an optical fiber to generate a ~10-fs probe pulse following recompression with prisms and gratings. Signals were modulated at 80 Hz, and data were collected with the use of a lock-in amplifier. Linearity of the data was confirmed using neutral density filters; the maximum observed change in transmission was typically 8%. Thirty spectra were collected at each time delay, and this cycle was repeated 20 times to afford the signal-averaged data.
18. A crystalline sample of $[Ru(bpy)_3](PF_6)_2$ was prepared by metathesis of commercially available $[Ru(bpy)_3]Cl_2$ (Aldrich) with NH_4PF_6 in aqueous solution, followed by two recrystallizations via diffusion of diethyl ether into CH_3CN that had been freshly distilled over CaH_2 and thoroughly degassed. Purity of the final product was checked by high-performance liquid chromatography, which gave a single peak, and elemental analysis indicating that the isolated compound was free of cocrystallized solvent. A static emission spectrum and nanosecond time-resolved emission data further confirmed the single-component nature of the sample. The sample was dissolved in dry, distilled CH_3CN and placed in a 0.2-mm pathlength cell (optical density = 0.6 at 475 nm). Absorption spectra of the sample measured before and after collection of a full data set were completely superimposable, indicating that there had been no significant photodegradation of the compound over the course of the experiment. Independent measurements made on different samples gave identical results. Data collected on the pure CH_3CN solvent showed signals attributable to cross-phase modulation between the pump and probe beams, but the relative amplitude of these signals were only about 10 to 15% that of $[Ru(bpy)_3]^{2+}$ and do not significantly affect the data illustrated in Fig. 2.
19. N. H. Damrauer, T. R. Boussie, M. Devenney, J. K. McCusker, unpublished results.
20. N. Sutin and C. Creutz, *Adv. Chem. Ser.* **168**, 1 (1978); N. Sutin, *Photochemistry* **80**, 97 (1979); C. Creutz, M. Chou, T. L. Netzel, M. Okumura, N. Sutin, *J. Am. Chem. Soc.* **102**, 1309 (1980).
21. It is difficult to assess vibrational relaxation dynamics given the broad, somewhat featureless nature of electronic absorption spectra. However, because charge-transfer spectra are particularly sensitive to changes in molecular structure, it is reasonable to assume that most of the structural rearrangement in the system is complete by $\Delta t = 300$ fs.
22. S. J. Rosenthal, X. Xie, M. Du, G. Fleming, *J. Chem. Phys.* **95**, 4715 (1991).
23. P. V. Kumar and M. Maroncelli, *ibid.* **103**, 3038 (1995) and references therein; M. Maroncelli, *ibid.* **94**, 2084 (1991); D. McMorrow and W. T. Lotshaw, *ibid.* **95**, 10395 (1991).
24. Y. K. Shin, B. S. Brunschwig, C. Creutz, N. Sutin, *J. Phys. Chem.* **100**, 8157 (1996) and references therein.
25. Although there is nothing known about the vibrational modes which couple to the $^1MLCT \rightarrow {}^3MLCT$ conversion, it is known that the C–C stretch of the bpy ring ($\hbar\omega \approx 1400\ cm^{-1}$) is strongly coupled to the $^3MLCT \rightarrow {}^1A_1$ relaxation process.
26. A similar proposal has been put forth to explain ultrafast $^1MLCT \rightarrow {}^5T_2$ conversion in a spin-crossover complex, although the time resolution was insufficient to observe the actual formation of the low-energy excited state. See J. K. McCusker, *et al*., *J. Am. Chem. Soc.* **115**, 298 (1993).
27. A. Vlcek Jr., *Chemtracts-Inorg. Chem.* **5**, 92 (1993).
28. This research was supported by the University of California (J.K.M.), the ACS-PRF grant 31016-G6 (J.K.M.), and the U.S. Department of Energy, contract DE-AC0376SF00098 (C.V.S.). G.C. acknowledges support from a NATO fellowship.

23 July 1996; accepted 29 October 1996

Effects of Monomer Structure on Their Organization and Polymerization in a Smectic Liquid Crystal

C. Allan Guymon, Erik N. Hoggan, Noel A. Clark, Thomas P. Rieker, David M. Walba, Christopher N. Bowman*

Photopolymerizable diacrylate monomers dissolved in fluid-layer smectic A and smectic C liquid crystal (LC) hosts exhibited significant spatial segregation and orientation that depend strongly on monomer structure. Small, flexible monomers such as 1,6-hexanediol diacrylate (HDDA) oriented parallel to the smectic layers and intercalated, whereas rod-shaped mesogen-like monomers such as 1,4-di-(4-(6-acryloyloxyhexyloxy)benzoyloxy)-2-methylbenzene (C6M) oriented normal to the smectic layers and collected within them. Such spatial segregation caused by the smectic layering dramatically enhanced photopolymerization rates; for HDDA, termination rates were reduced, whereas for C6M, both the termination and propagation rates were increased. These polymerization precursor structures suggest novel materials-design paradigms for gel LCs and nanophase-separated polymer systems.

In pursuit of novel LC phase behavior and properties, a number of polymer-LC composites have been developed. Some composites make use of LC polymers (*1*), whereas others are formed by phase separation of the polymer and LC to produce LC droplets [polymer-dispersed LCs (PDLCs) (*2, 3*)]. Another group of these composites that show great promise is formed by the polymerization of monomer solutes in an LC solvent (*4*). These polymer-LC gel systems can yield electro-optically bistable chiral nematic devices [polymer-stabilized LCs (PSLCs) (*5*)] and ferroelectric LC gels [(PSFLCs) (*6, 7*)], which combine fast electro-optic response (*8*) with polymer-induced mechanical stabilization (*9*). Research to date on the formation and structure of polymer-LC gels has focused on the macroscopic phase behavior and optical properties of the resulting composites (*10*). Little is known, however, about the roles that the monomer segregation and subsequent polymerization behavior play on the ultimate performance of the polymer-LC gel.

We report results on the effect of diacrylate monomer structure on the spatial organization of monomer-LC mixtures prior to polymerization and thus the effect of monomer segregation and structure on polymerization kinetics. This work was initially motivated by observations of a dramatically enhanced rate of photopolymerization of LC acrylate monomers (*11*) and decreased termination rate (*12*) in LC phases, which suggests that the inherent order in LCs can significantly alter chemical reaction behavior and kinetics (*13*). The fluidlike environment in LCs not only permits molecular motion, diffusion, and chemical reaction, but also is both spatially anisotropic (orientational ordered) and spatially inhomogeneous (for example, layered). We find distinctive structure-dependent positional and orientational ordering of the monomers in which small flexible monomers intercalate between smectic layers and mesogenic

C. A. Guymon, E. N. Hoggan, C. N. Bowman, Department of Chemical Engineering, University of Colorado, Boulder, CO 80309–0424, USA.
N. A. Clark, Department of Physics, University of Colorado, Boulder, CO 80309–0390, USA.
T. P. Rieker, Department of Chemical and Nuclear Engineering, Center for Micro-Engineered Materials, University of New Mexico, Albuquerque, NM 87106, USA.
D. M. Walba, Department of Chemistry, University of Colorado, Boulder, CO 80309–0215, USA.
*To whom correspondence should be addressed.